Lorenz System

Universiteit Utrecht

Name: Samantha van Wijk

Student number: 2708132

Course: Inleiding niet-lineaire dynamische systemen

1 Introduction

Edward N. Lorenz's research on atmospheric convection and weather forecasting in the early 1960s is the source of the Lorenz-63 equations. As a meteorologist at the Massachusetts Institute of Technology, Lorenz was interested in the actual quality of weather predictability [5]. Weather models of the time included numerous equations derived from fluid dynamics and were extremely complex. Lorenz was wondering if basic atmospheric dynamics could still be described by simpler models.

Lorenz chose to focus on Rayleigh-Bénard convection, a physical situation where a thin layer of fluid is heated from below and cooled from above. When the temperature differences between the bottom and top surfaces is low, heat is transported solely through conduction. However, when the temperature difference exceeds a particular point, convection takes over: warm fluid rises, cold fluid sinks, and regular flow patterns such as convection rolls develop. This process was previously explained theoretically using partial differential equations developed on the basis of the Navier-Stokes equations.

Lorenz's work was based on a previous model developed by Saltzman, who used Fourier series to describe this convective flow. In Saltzman's model, temperature and velocity fields are involved in partial differential equations. Lorenz maintained only the three most significant modes of the Fourier expansion in order to make the problem manageable. The original system was drastically simplified to three ordinary differential equations that only depended on time. The resulting variables represent the intensity of convection and the fluid's temperature variations, both horizontally and vertically. The fluid's physical properties and the strength of the thermal forcing are described by the parameters $\sigma, r,$ and b, which are positive parameters.The Lorenz system

$$\begin{cases} \dot{x} = \sigma(y - x) \\ \dot{y} = rx - y - xz \\ \dot{z} = -bz + xy \end{cases}$$

is made up of these three equations, each of which describes a different aspect of the relationship between flow and temperature. The first equation describes the convective flow intensity (x). The second equation describes the horizontal temperature variation (y). It decreases by damping and interaction with the vertical variation in temperature through the nonlinear term xz, while it increases by convection through the term rx. The third equation demonstrates the vertical temperature variation z, which is decreased by the linear decay term bz and increased by the product xy, which represents the connection between flow and temperature. These nonlinear interaction terms are the reason of the system's complicated behavior.

However, the most significant finding came from Lorenz's numerical experiments rather than the derivation itself. In 1961, Lorenz was utilizing twelve differential equations to simulate an atmospheric model on a computer. He once restarted a simulation with values printed from a previous run. Compared to the values that the computer internally kept, these values were rounded to fewer decimal points. Even though there was minimal variation in the original data, the new simulation soon produced an entirely different outcome. This unexpected result demonstrated how sensitive the system was to start conditions. Over time, even small variations in the initial state could increase exponentially and result in drastically different long-term behavior. This phenomena became known as the butterfly effect, which holds that a relatively slight disturbance, like as the flap of a butterfly's wings, can eventually lead to large-scale effects, such as altered weather patterns. In the Lorenz system, two trajectories that start arbitrarily close to one another will eventually separate and follow entirely distinct paths, while they obey the same deterministic equations.

Lorenz researched the long-term behavior of the three-dimensional system for particular parameter values (most commonly $\sigma = 10, b = 8/3,$ and $r = 28$) and discovered that solutions do not settle into fixed points or periodic orbits. Rather, a complex butterfly-shaped set—now termed as the Lorenz attractor—attracts a large number of trajectories. The motion on this attractor is chaotic; it is deterministic and bounded, but because of its sensitive dependency on initial conditions, it is unpredictable over time.

Thus, a combination of numerical experimentation, mathematical simplification, and physical modeling led to the development of the Lorenz-63 equations. They disclose a fundamental limit to predictability and demonstrate how a relatively simple system of three standard differential equations can already represent key aspects of atmospheric dynamics. This realization significantly influenced scientists' understanding of complicated dynamical systems and provided the basis for chaos theory.

2 Equilibria

To work with this system it is important to start by analyzing the stability of equilibria in the system. In particular, you can derive a condition for a nonzero equilibrium to have a Hopf bifurcation.

The equilibria of the system are the points for which $\dot{x} = \dot{y} = \dot{z} = 0$, so in this case

$$\begin{cases} \sigma(y - x) & = 0 \\ rx - y - xz & = 0 \\ -bz + xy & = 0. \end{cases}$$

When we rewrite these equations, we see that in order to have an equilibrium, we need to meet the conditions

$$\begin{aligned} y &= x \\ x(r - 1 - z) &= 0 \\ x^2 &= bz. \end{aligned}$$

Using this, we see that for every equilibrium the x-coordinate and the y-coordinate are equal, and that $x = \pm\sqrt{bz}$. Next, we see that one equilibrium is at $x = 0$, thus $y = 0$ and $z = 0$. Giving the equilibrium $E_0 = (0, 0, 0)$. The other equilibria are for $z = r - 1$, $x = y = \pm\sqrt{b(r-1)}$. These are the other two equilibria: $E_\pm = (\pm\sqrt{b(r-1)}, \pm\sqrt{b(r-1)}, r - 1)$. For $E_\pm$ to exist, we notice, since $b > 0$, that r should be greater than 1. This is because if $r < 1$, we get a negative square root, and for $r = 1$, we get E_0.

Next, we calculate the Jacobian matrix, which describes the linearization of the system around an equilibrium and allows us to determine local stability by analyzing the eigenvalues of the linearized flow. The Jacobian matrix is determined as follows.

$$J_{(x,y,z)} = \begin{pmatrix} \frac{\partial \dot{x}}{\partial x} & \frac{\partial \dot{x}}{\partial y} & \frac{\partial \dot{x}}{\partial z} \\ \frac{\partial \dot{y}}{\partial x} & \frac{\partial \dot{y}}{\partial y} & \frac{\partial \dot{y}}{\partial z} \\ \frac{\partial \dot{z}}{\partial x} & \frac{\partial \dot{z}}{\partial y} & \frac{\partial \dot{z}}{\partial z} \end{pmatrix} = \begin{pmatrix} -\sigma & \sigma & 0 \\ r - z & -1 & -x \\ y & x & -b \end{pmatrix}.$$

For E_0, we find:

$$J_{(0,0,0)} = \begin{pmatrix} -\sigma & \sigma & 0 \\ r & -1 & 0 \\ 0 & 0 & -b \end{pmatrix}.$$

The eigenvalues of the Jacobian can be found by solving;

$$\det(J - \lambda I) = 0.$$

We first determine $J - \lambda I$.

$$J - \lambda I = \begin{pmatrix} -\sigma - \lambda & \sigma & 0 \\ r & -1 - \lambda & 0 \\ 0 & 0 & -b - \lambda \end{pmatrix}.$$

Since the matrix is a block-diagonal, we can split the determinant:

$$\det(J - \lambda I) = (-b - \lambda) \det \begin{pmatrix} -\sigma - \lambda & \sigma \\ r & -1 - \lambda \end{pmatrix}.$$

When we work this out we find:

$$\begin{aligned}(-b-\lambda)\det\begin{pmatrix}-\sigma-\lambda & \sigma\\ r & -1-\lambda\end{pmatrix} &= (-b-\lambda)((-\sigma-\lambda)(-1-\lambda)-\sigma r)\\ &= (-b-\lambda)((\sigma+\lambda)(1+\lambda)-\sigma r)\\ &= (-b-\lambda)(\lambda^2+(\sigma+1)\lambda+\sigma(1-r))=0.\end{aligned}$$

This gives the following eigenvalues:

$$\lambda_1=-b,\quad \lambda_{2,3}=\frac{-(\sigma+1)\pm\sqrt{(\sigma+1)^2-4\sigma(1-r)}}{2}.$$

Now that we have computed the eigenvalues, we can determine the stability of this equilibirium.

1. For $r<1$, all eigenvalues are negative, indicating that E_0 is asymptotically stable.
2. For $r=1$, one eigenvalue crosses zero, a supercritical pitchfork bifurcation occurs [4].
3. For $r>1$, one eigenvalue is positive, so E_0 is a unstable saddle.

Next, we look at the equilibrium E_+. Since the equilibria $E_\pm$ are symmetrical, we can conclude that they have identical eigenvalues and stability properties. So, the stabilities we have will determine for E_+ are the same as for E_-. The Jacobian matrix of E_+ gives:

$$J_{(\sqrt{b(r-1)},\sqrt{b(r-1)},r-1)}=\begin{pmatrix}-\sigma & \sigma & 0\\ 1 & -1 & -\sqrt{b(r-1)}\\ \sqrt{b(r-1)} & \sqrt{b(r-1)} & -b\end{pmatrix}.$$

We can use the characteristic polynomial to determine the eigenvalues of the matrix, for any 3×3 matrix J, this equation has the following form;

$$\lambda^3+a_1\lambda^2+a_2\lambda+a_3=0.$$

For which;

$$\begin{aligned}a_1 &= -Tr(J)\\ &= -(-b-\sigma-1)\\ &= b+\sigma+1,\\ a_2 &= \begin{vmatrix}J_{11} & J_{12}\\ J_{21} & J_{22}\end{vmatrix}+\begin{vmatrix}J_{11} & J_{13}\\ J_{31} & J_{33}\end{vmatrix}+\begin{vmatrix}J_{22} & J_{23}\\ J_{32} & J_{33}\end{vmatrix}\\ &= \begin{vmatrix}-\sigma & \sigma\\ 1 & -1\end{vmatrix}+\begin{vmatrix}-\sigma & 0\\ \sqrt{b(r-1)} & -b\end{vmatrix}+\begin{vmatrix}-1 & -\sqrt{b(r-1)}\\ \sqrt{b(r-1)} & -b\end{vmatrix}\\ &= (\sigma-\sigma)+(\sigma b-0)+b+b(r-1)\\ &= \sigma b+b+br-b\\ &= b(r+\sigma),\\ a_3 &= -\det(J)\\ &= -(-\sigma(b+b(r-1))-\sigma(-b+b(r-1))+0\\ &= -(-\sigma br+2\sigma b-\sigma br)\\ &= 2\sigma br-2\sigma b\\ &= 2\sigma b(r-1).\end{aligned}$$

We can fill in these values into the equation:

$$\lambda^3 + (\sigma + b + 1)\lambda^2 + b(r + \sigma)\lambda + 2\sigma b(r - 1) = 0.$$

All the eigenvalues have a negative real part if

$$a_1 > 0, \qquad a_2 > 0, \qquad a_3 > 0, \qquad a_1 a_2 > a_3,$$

according to the Routh-Hurwitz stability criterion for third-order characteristic polynomials [7]. A Hopf bifurcation occurs when a pair of complex conjugate eigenvalues of the Jacobian crosses the imaginary axis, which happens when $a_1 a_2 = a_3$ is satisfied, for $a_1, a_2, a_3 > 0$. The transversality condition is satisfied since the real part of the complex eigenvalues crosses zero with nonzero speed as r varies. Hence, we determine the value of r for which $a_1 a_2 = a_3$ holds.

Thus, when we work

$$(\sigma + b + 1) \cdot b(r + \sigma) = 2\sigma b(r - 1)$$

out, you will get

$$\sigma r + \sigma^2 + br + \sigma b + r + \sigma = 2\sigma r - 2\sigma.$$

Freeing r, shows that a Hop bifurcation occurs when

$$r(\sigma + b + 1 - 2\sigma) = -2\sigma - \sigma^2 - \sigma b - \sigma$$
$$r_H = \frac{-\sigma(\sigma + b + 3)}{-\sigma + b + 1} = \frac{\sigma(\sigma + b + 3)}{\sigma - b - 1}$$

if $\sigma > b + 1$.

So r_H is the condition for both E_- and E_+ to have a Hopf bifurcation.

Using this value of r, can determine the stability of E_+, we again have three cases;

1. Case $1 < r < r_H$; for this case we see that $a_1, a_2, a_3 > 0$ and $a_1 a_2 > a_3$. This indicates an asymptotically stable equilibrium.
2. Case $r = r_H$; we found that $a_1 a_2 = a_3$, resulting in a Hopf bifurcation.
3. Case $r > r_H$; we have $a_1 a_2 < a_3$, which indicates an unstable equilibrium.

This change of stability is consistent with the Hopf bifurcation theorem, since the transversality condition is satisfied and a pair of complex conjugate eigenvalues crosses the imaginary axis with nonzero speed as the parameter r varies.

Thus, we see that the Lorenz-63 system undergoes a pitchfork bifurcation at $r = 1$, where the trivial equilibrium loses stability and two symmetric equilibria emerge. These nonzero equilibria are stable for $1 < r < r_H$, where

$$r_H = \frac{\sigma(\sigma + b + 3)}{\sigma - b - 1}, \qquad \sigma > b + 1.$$

At $r = r_H$, a Hopf bifurcation occurs as a complex conjugate pair of eigenvalues crosses the imaginary axis, destabilizing the equilibria and giving rise to oscillatory dynamics.

3 Hopf bifurcation

We will now dive deeper into the bifurcation and the type of it. The nature of the Hopf bifurcation can be determined by looking at the sign of the first Lyapunov coefficient. When two complex conjugate eigenvalues cross the imaginary axis, the Hopf bifurcation theorem ensures the presence of a branch of periodic solutions. However, it does not specify the stability of these solutions.

The first Lyapunov coefficient, which estimates the leading-order nonlinear effects on the oscillation amplitude near the bifurcation point, provides this information. The criticality of the Hopf bifurcation is specifically determined by the sign of the first Lyapunov coefficient: a positive value indicates a subcritical Hopf bifurcation, which is characterized by the presence of an unstable periodic orbit and a possibility for abrupt transitions to large-amplitude dynamics, while a negative value indicates a supercritical Hopf bifurcation, whereby a stable periodic orbit emerges as the equilibrium loses stability. In order to categorize the bifurcation in addition to understanding the qualitative behavior of solutions close to the critical parameter value, it is essential to compute this first Lyapunov coefficient.

3.1 General formula for the Lyapunov coefficient

First, we will take a look at the general formula to determine the first Lyapunov coefficient, and later on we will apply this for the Lorenz-63 system. The general formula is taken from Shilnikov et al. (2001),in Methods of Qualitative Theory in Nonlinear Dynamics, Part II for the first Lyapunov value weak focus of the three-dimensional system

$$\dddot{\xi} + a_1\ddot{\xi} + a_2\dot{\xi} + a_3\xi = f(\xi, \dot{\xi}, \ddot{\xi})$$

where f represents the nonlinear part of the system. We assume that f is sufficiently smooth and that its Taylor expansion at the origin starts with quadratic terms, so that the linearization fully determines the local stability. The coefficients a_1, a_2, a_3 are assumed to satisfy the relation

$$a_1 a_2 = a_3, \qquad a_2 > 0,$$

which ensures that the linearized system has a pair of purely imaginary eigenvalues and thus lies on a Hopf bifurcation boundary. To rewrite the system as a first-order system, we introduce the variables $U \equiv (u_1, u_2, u_3) = (\xi, \dot{\xi}, \ddot{\xi})$, which allows us to express the equation in vector form as

$$\dot{U} = AU + f(U) \cdot \begin{pmatrix} 0 \\ 0 \\ 1 \end{pmatrix}$$

where the linear part is given by the Lesley matrix

$$A = \begin{pmatrix} 0 & 1 & 0 \\ 0 & 0 & 1 \\ -a_1 a_2 & -a_2 & -a_1 \end{pmatrix}.$$

The spectrum of the matrix A consists of one real eigenvalue $-a_1$ and a complex conjugate pair $\pm i\omega$, where $\omega^2 = a_2$. Thus, the linearized system has a two dimensional center subspace associated with the imaginary eigenvalues and a one-dimensional stable subspace corresponding to the negative eigenvalue. The associated $\pm i\omega$ are

$$\begin{pmatrix} 1 \\ i\omega \\ -a_2 \end{pmatrix}, \qquad \begin{pmatrix} 1 \\ -i\omega \\ -a_2 \end{pmatrix}, \qquad \begin{pmatrix} 1 \\ -a_1 \\ a_1^2 \end{pmatrix},$$

and the eigenvectors of the adjoint matrix are respectively given by

$$\begin{pmatrix} a_1\omega \\ \omega - ia_1 \\ -i \end{pmatrix}, \qquad \begin{pmatrix} a_1\omega \\ \omega + ia_1 \\ i \end{pmatrix}, \qquad \begin{pmatrix} a_2 \\ 0 \\ 1 \end{pmatrix}.$$

Using these eigenvectors, we introduce new coordinates $r \in \mathbb{R}^1$ and $s \in \mathbb{C}^1$, corresponding to the stable and center directions, respectively. The transformation is defined by

$$U = r \begin{pmatrix} 1 \\ -a_1 \\ a_1^2 \end{pmatrix} + s \begin{pmatrix} 1 \\ i\omega \\ -a_2 \end{pmatrix} + s^* \begin{pmatrix} 1 \\ -i\omega \\ -a_2 \end{pmatrix}.$$

Here, z^* denotes the complex conjugate of z, ensuring that the state vector U remains real. This change of variables diagonalizes the linear part of the system and separates the dynamics along the center and stable directions. The evolution equations for r and s are obtained by projecting $\dot{U}$ onto the adjoint eigenvectors. This yields

$$\dot{r} = \frac{1}{a_2 + a_1^2}(a_2\dot{u}_1 + \dot{u}_3), \qquad \dot{s} = \frac{1}{2a_1\omega}(a_1\omega\dot{u}_1 + (\omega - ia_1)\dot{u}_2 - i\dot{u}_3).$$

Substituting the nonlinear terms and expanding, we arrive at the system

$$\begin{aligned} \dot{r} &= -a_1 r + \alpha_1 s^2 + \alpha_2 z z^* + \cdots, \\ \dot{s} &= i\omega s + \beta_1 z^2 + \beta_2 z z^* - \beta_1^* {z^*}^2 + \gamma r s - \gamma^* r s^* + \delta z^2 z^* + \cdots, \end{aligned} \tag{1}$$

where higher order terms, which are indicated by the dots, do not affect the computation of the first Lyapunov coefficient. To compute the coefficients appearing above, we expand the nonlinearity up to third order:

$$f(U) = \sum c_{kj} y_j y_k + \sum d_{kjl} y_k y_j y_l + \cdots.$$

Substituting this expansion into the expressions for $\dot{r}$ and $\dot{s}$, one obtains explicit formulas for the coefficients α, β, γ and δ given by:

$$\begin{aligned} (a_2 + a_1^2)\alpha_1 &= 2ia_1\omega\beta_1 = \sum c_{kj}(i\omega)^{k+j-2}, \\ (a_2 + a_1^2)\alpha^2 &= 2ia_1\omega\beta_2 = -\sum((-1)^k + (-1)^j)c_{kj}(i\omega)^{k+j-2}, \\ \gamma &= \frac{1}{2}\sum c_{kj}((-a_1)^{k-2}(i\omega)^{j-2} + (-a_1)^{j-2}(i\omega)^{k-2}), \\ \delta &= -\frac{1}{2a_1 a_2^2}\sum d_{kjl}(i\omega)^{k+j+l}((-1)^k + (-1)^j + (-1)^l). \end{aligned}$$

These coefficients encode how the nonlinear terms interact with the critical eigenmodes. The center manifold of the system (1) is given by

$$r = \frac{\alpha_1}{a_1 + i\omega}s^2 + \frac{\alpha_2}{a_1}ss^* + \cdots,$$

which expresses the stable variable r as a function of the center variables. Restricting the dynamics to this manifold eliminates the stable direction and yields an effective equation on the center manifold:

$$\dot{s} = i\omega s + \beta_1 s^2 + \beta_2 ss^* - \beta_1^* {s^*}^2 + \left(\gamma\frac{\alpha_2}{a_1} - \gamma^*\frac{\alpha_1}{a_1 + i\omega} + \delta\right)s^2 s^* + \cdots.$$

Finally, a near-identity normalizing transformation

$$s_{new} = s + i\frac{\beta_1}{\omega}s^2 - i\frac{\beta_2}{\omega}ss^* + i\frac{\beta_1^*}{3\omega}{s^*}^2$$

removes all quadratic terms. As a result, the system on the center manifold takes the normal form

$$\dot{s} = i\omega s + (L_1 + i\Omega_1)s^2 s^* + \cdots,$$

where

$$L_1 + i\Omega_1 = \frac{i}{\omega}\left(\beta_1\beta_2 - |\beta_1|^2 - \frac{2}{3}|\beta_2|^2\right) + \gamma\frac{\alpha_2}{a_1} - \gamma^*\frac{\alpha_1}{a_1 + i\omega} + \delta.$$

By definition, the real part L_1 is the first Lyapunov coefficient.

3.2 Lyapunov coefficient for the Lorenz System

Now, we will apply this general algorithm developed in section 3.1 to determine the nature of the Hopf bifurcation of the nontrivial equilibria of the Lorenz-63 system. As discussed earlier, the computation of the first Lyapunov coefficient allows us to decide whether the Hopf bifurcation is subcritical or supercritical. As a reminder, we consider the Lorenz system

$$\begin{cases} \dot{x} = \sigma(y - x) \\ \dot{y} = rx - y - xz \\ \dot{z} = -bz + xy \end{cases}$$

and we will focus on the equilibria $E_\pm = (\pm\sqrt{b(r-1)}, \pm\sqrt{b(r-1)}, r-1)$, which exist for $r > 1$. Following the approach outlined in the general case, we first reduce the Lorenz system to a single third-order differential equation for the variable x. This reduction is useful because it allows us to bring the system into the standard form

$$\dddot{\xi} + P\ddot{\xi} + Q\dot{\xi} + R\xi = f(\xi, \dot{\xi}, \ddot{\xi}), \tag{2}$$

to which the Lyapunov coefficient formula derived earlier applies.

Carrying out the elimination procedure, the Lorenz system can be rewritten as

$$\dddot{x} + (\sigma + b + 1)\ddot{x} + b(1 + \sigma)\dot{x} + b\sigma(1 - r)x = \frac{(1 + \sigma)\dot{x}^2}{x} + \frac{\dot{x}\ddot{x}}{x} - x^2\dot{x} - \sigma x^3. \tag{3}$$

To analyze the Hopf bifurcation at $E_\pm$, we translate the equilibrium to the origin by introducing the new variable

$$\xi = x - x_0, \qquad x_0 = \pm\sqrt{b(r-1)}.$$

As in the general theory, only quadratic and cubic terms of the nonlinearity are required for the computation of the first Lyapunov coefficient. Therefore, higher-order terms are neglected.

After substitution and expansion, equation (3) indeed takes the form

$$\dddot{\xi} + (\sigma + b + 1)\ddot{\xi} + [b(1 + \sigma) + x_0^2]\dot{\xi} + [b\sigma(1 - r) + 3\sigma x_0^2]\xi = f(\xi, \dot{\xi}, \ddot{\xi}), \tag{4}$$

where the nonlinear part is given by

$$f(\xi, \dot{\xi}, \ddot{\xi}) = -3\sigma x_0\xi^2 - 2x_0\xi\dot{\xi} + \frac{1 + \sigma}{x_0}\dot{\xi}^2 + \frac{1}{x_0}\dot{\xi}\ddot{\xi} - \sigma\xi^3 - \xi^2\dot{\xi} - \frac{1 + \sigma}{x_0^2}\xi\dot{\xi}^2 - \frac{1}{x_0^2}\xi\dot{\xi}\ddot{\xi} + \cdots.$$

Comparing equation (4) with the general form studied previously, we identify

$$\begin{aligned} R &= b\sigma(1 - r) + 3\sigma x_0^2, \\ Q &= b(1 + \sigma) + x_0^2, \\ P &= \sigma + b + 1. \end{aligned}$$

Introducing the state vector

$$U = (\xi, \dot{\xi}, \ddot{\xi})^T \in \mathbb{R}^3,$$

the equation can be rewritten as a first-order system

$$\dot{U} = AU + F(U),$$

Therefore, we define $U = \begin{pmatrix} u_1 \\ u_2 \\ u_3 \end{pmatrix} = \begin{pmatrix} \xi \\ \dot{\xi} \\ \ddot{\xi} \end{pmatrix}$. We then see:

$$\begin{aligned} \dot{u}_1 &= \dot{\xi} = u_2, \\ \dot{u}_2 &= \ddot{\xi} = u_3, \\ \dot{u}_3 &= \dddot{\xi}. \end{aligned}$$

For $\dot{u}_3$, we can rewrite the equation, in order to have $\dddot{\xi}$ on the left side of the equation and the rest of the terms on the right side. This gives us:

$$\begin{aligned} \dot{u}_3 = \dddot{\xi} &= -(\sigma + b + 1)\ddot{\xi} - [b(1+\sigma) + x_0^2]\dot{\xi} - [b\sigma(1-r) + 3\sigma x_0^2]\xi + f(\xi, \dot{\xi}, \ddot{\xi}) \\ &= -P\ddot{\xi} - Q\dot{\xi} - R\xi + f(\xi, \dot{\xi}, \ddot{\xi}). \end{aligned}$$

We can substitute $\xi = u_1$, $\dot{\xi} = u_2$ and $\ddot{\xi} = u_3$, which gives:

$$\dot{u}_3 = -Ru_1 - Qu_2 - Pu_3 + f(u_1, u_2, u_3).$$

We then have the following system:

$$\begin{cases} \dot{u}_1 = u_2 \\ \dot{u}_2 = u_3 \\ \dot{u}_3 = -Ru_1 - Qu_2 - Pu_3 + f(u_1, u_2, u_3) \end{cases}$$

Thus we see that $\dot{U}$ becomes:

$$\begin{aligned} \dot{U} &= \begin{pmatrix} 0 & 1 & 0 \\ 0 & 0 & 1 \\ -R & -Q & -P \end{pmatrix} U + \begin{pmatrix} 0 \\ 0 \\ f(u_1, u_2, u_3) \end{pmatrix} \\ &= \begin{pmatrix} 0 & 1 & 0 \\ 0 & 0 & 1 \\ -(b\sigma(1-r) + 3\sigma x_0^2) & -(b(1+\sigma) + x_0^2) & -(\sigma + b + 1) \end{pmatrix} U + \begin{pmatrix} 0 \\ 0 \\ f(u_1, u_2, u_3) \end{pmatrix}. \end{aligned}$$

Having rewritten the Lorenz system in the canonical form $\dot{U} = AU + F(U)$, all assumptions of the general Hopf bifurcation framework developed in section 3.1 are satisfied. On the stability boundary, the linearization A has one negative real eigenvalue; $-P = -(\sigma + b + 1)$ and a pair of purely imaginary eigenvalues $\pm i\omega$, where $\omega^2 = Q = b(1+\sigma) + x_0^2 = b(\sigma + r)$.
The associated eigenvectors are

$$\begin{pmatrix} 1 \\ -(\sigma + b + 1) \\ (\sigma + b + 1)^2 \end{pmatrix}, \qquad \begin{pmatrix} 1 \\ i\sqrt{b(1+\sigma) + x_0^2} \\ -(b(1+\sigma) + x_0^2) \end{pmatrix}, \qquad \begin{pmatrix} 1 \\ -i\sqrt{b(1+\sigma) + x_0^2} \\ -(b(1+\sigma) + x_0^2) \end{pmatrix},$$

and the eigenvectors of the adjoint matrix are respectively given by

$$\begin{pmatrix} b(1+\sigma) + x_0^2 \\ 0 \\ 1 \end{pmatrix}, \qquad \begin{pmatrix} (\sigma + b + 1)\sqrt{b(1+\sigma) + x_0^2} \\ \sqrt{b(1+\sigma) + x_0^2} - i(\sigma + b + 1) \\ -i \end{pmatrix}, \qquad \begin{pmatrix} (\sigma + b + 1)\sqrt{b(1+\sigma) + x_0^2} \\ \sqrt{b(1+\sigma) + x_0^2} + i(\sigma + b + 1) \\ i \end{pmatrix}.$$

Using these computed eigenvectors of the adjoint matrix, we are able to find the first Lyapunov coefficient. Fortunately, these nuumerical calculations were also done by Shilnikov et al (2001). Using the method from above, they have determined that with everything we have just computed and the fact that the stability boundary for both E_+ and E_- is given by

$$r = \frac{\sigma(\sigma + b + 3)}{\sigma - b - 1},$$

the first Lyapunov value is

$$L_1 = b[p^3 q(p^2 + q)(p^2 + 4q)(\sigma - b - 1)]^{-1} B,$$

where

$$B = [9\sigma^4 + (20 - 18b)\sigma^3 + (20b^2 + 2b + 10)\sigma^2 - (2b^3 - 12b^2 - 10b + 4) - b^4 - 6b^3 - 12b^2 - 10b - 3].$$

We will now analyse the sign of the first Lyapunov coefficient L_1. On the Hopf stability boundary, the parameters satisfy

$$r = \frac{\sigma(\sigma + b + 3)}{\sigma - b - 1},$$

which implies the necessary inequality $\sigma > b + 1$. To make this explicit in the expression for L_1, we introduce the shifted parameter

$$\sigma = b + 1 + \sigma^*, \qquad \sigma^* > 0.$$

Substituting this expression into the polynomial B, one finds that B can be written as a polynomial. We use that;

$$\begin{aligned}
&\sigma = b + 1 + \sigma^*, \qquad \sigma^* > 0, \\
&\sigma^2 = (b + 1 + \sigma^*)^2 = \sigma^{*2} + 2(b + 1)\sigma^* + (b + 1)^2, \\
&\sigma^3 = \sigma^{*3} + 3(b + 1)\sigma^{*2} + 3(b + 1)^2\sigma^* + (b + 1)^3, \\
&\sigma^4 = \sigma^{*4} + 4(b + 1)\sigma^{*3} + 6(b + 1)^2\sigma^{*2} + 4(b + 1)^3\sigma^* + (b + 1)^4.
\end{aligned}$$

Which gives us:

$$B = c_4\sigma^{*4} + c_3(b)\sigma^{*3} + c_2(b)\sigma^{*2} + c_1(b)\sigma^* + c_0(b),$$

where the coefficient after straightforward algebra are:

$$\begin{aligned}
c_4 &= 9, \\
c_3(b) &= 36(b + 1) + 20 - 18b = 18b + 56, \\
c_2(b) &= 54(b + 1)^2 + 3(20 - 18b)(b + 1) + (20b^2 + 2b + 10) \\
&= 20b^2 + 92b + 136, \\
c_1(b) &= 36(b + 1)^3 + 3(20 - 18b)(b + 1)^2 + 2(20b^2 + 2b + 10)(b + 1) - (2b^3 - 2b^2 - 10b + 4) \\
&= 2b^3 + 54b^2 + 162b + 132.
\end{aligned}$$

So, we see that B can be written as a polynomial in σ^* and b whose coefficients are all strictly positive. Since the remaining prefactor in the expression for L_1 is also positive for $b > 0$ and $\sigma > b + 1$, it follows that if $\sigma^* > 0$ and $b > 0$, then $L_1 > 0$ for all admissible parameter values on the stability boundary. Thus, both equilibria $E_\pm$ are unstable on the stability boundary. Therefore, the corresponding Andronov-Hopf bifurcation of $E_\pm$ is always subcritical.

4 Global bifurcations of the system

In this final section we want to describe the global bifurcations of the system leading to the Lorenz strange attractor and related 1D dynamics. Several figures in this section are adapted from Guckenheimer and Holmes (1983) [2]. In these figures, r represents the equilibrium E_0, while q^- and q^+ represent the stable equilibria E_- and E_+, respectively. We consider the Lorenz system with the standard parameter values

$$\sigma = 10, \qquad b = \tfrac{8}{3},$$

and use the Rayleigh number r as the control. The sequence of global bifurcations leading to the Lorenz strange attractor cannot be fully understood using local bifurcation theory alone. Instead, a geometric approach based on one-dimensional return maps is most helpful. This approach was developed by Kaplan and Yorke (1979) [8] and given a rigorous geometric formulation by Guckenheimer and Holmes (1983) [2].

As we have seen before, for $r \leq 1$, the Lorenz system has a single equilibrium at the origin $E_0 = (0, 0, 0)$, which is globally asymptotically stable. At $r = 1$, a pitchfork bifurcation occurs: the origin loses stability and two symmetric equilibria appear:

$$E_\pm = (\pm\sqrt{b(r-1)}, \pm\sqrt{b(r-1)}, r-1).$$

We can show this in a bifurcation diagram as follows:

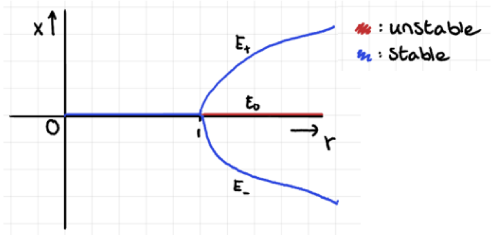

Figure 1: Bifurcation diagram

For $1 < r < r_t$, where $r_t \approx 13.926$ is numerically found by Guckenheimer and Holmes (1983). The equilibria $E_\pm$ are asymptotically stable, while the origin is a saddle with a one-dimensional unstable manifold. Trajectories starting near the origin move away along this unstable direction, while those near $E_\pm$ are attracted to these stable equilibria. In this range, all trajectories eventually settle at one of the stable equilibria. There is no chaotic behavior yet (see Figure 2a).

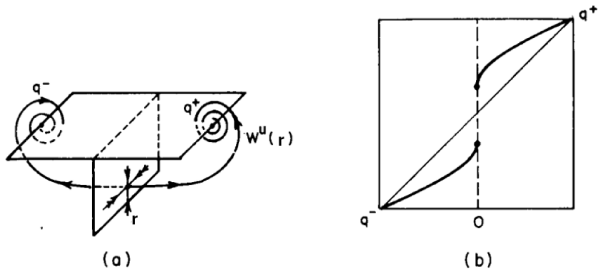

Figure 2: The Lorenz system for $r \approx 10, \sigma = 10, b = \frac{8}{3}$. (a) The flow; (b) the return map f_r (taken from [2]).

As r increases, the global structure of the flow changes. To study this, we introduce a Poincaré section Σ, a plane transverse to the flow near $z = r - 1$. We record where trajectories intersect this plane. Mapping

each intersection to the next defines the Lorenz return map

$$f_r : \Sigma \to \Sigma,$$

with Σ being 2 dimensional. This map captures how points move along the unstable direction. Herefore, we use a strong stable foliation, which lets you collapse many trajectories that rapidly converge to each other into a single one, greatly simplifying the dynamics, this is what we call leaves. Differences along the stable directions die out quickly. Therefore, the long-term behavior of the system is largely determined by the two-dimensional map (Figure 2b). This map captures the evolution along the unstable direction: it shows how a small displacement along this direction is stretched, folded, and shifted by the flow over time. Differences along the stable directions quickly die out due to strong contraction, so the long-term behavior of the system is essentially determined by how points move under f_r. In other words, by studying this simple one-dimensional map, we can understand and predict the skeleton of the complex three-dimensional dynamics of the Lorenz system.

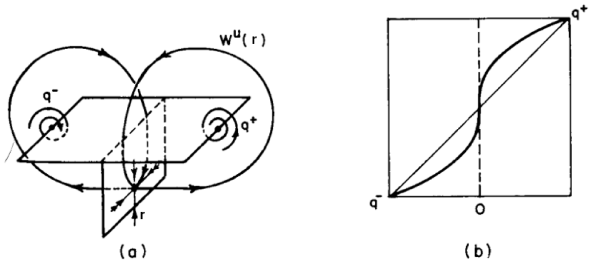

Figure 3: The Lorenz system for $r = r_t \approx 13.926$. (a) The flow; (b) the map f_r (taken from [2]).

When r reaches a critical value, at around $r = r_t$, a bifurcation occurs, in which the unstable manifold of the origin forms homoclinic orbits, meaning trajectories leave the origin E_0 along the unstable direction and return to it along the stable direction, see Figure 3. This S-shaped curve indicates the stretching and folding of trajectories. It lays so close together because even a slight change in r can decide left or right. The middle portion of the S-shaped curve in Figure 3b corresponds to an unstable periodic orbit of the map f_r. For $r > r_t$, this orbit splits into two separate branches, r^- and r^+, representing trajectories that initially move to the left or right before returning along the stable direction. This splitting, combined with the steep slope of the map, illustrates how small differences in initial conditions can lead to divergent outcomes, laying the groundwork for chaotic dynamics.

Increasing r even further, so for $r_t < r < r_a \approx 24.06$, as is done in Figure 4, the homoclinic bifurcation is followed by flows for which each branch of the unstable manifold crosses to the opposite side of the stable manifold of r as it descends for the first time. Hereby, is r_a also numerically found according to [2]. Near the homoclinic bifurcation, the slope of f_r becomes very steep near a discontinuity point d, indicating strong stretching in the dynamics.

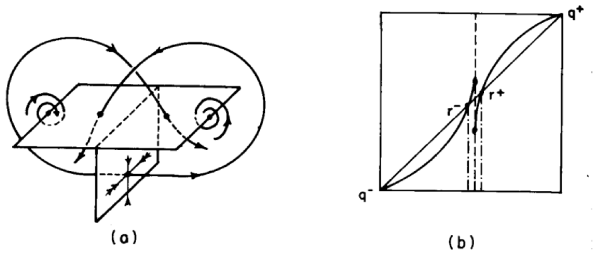

Figure 4: The Lorenz system for $r > r_t$. (a) The flow; (b) the map f_r (taken from [2]).

Two unstable fixed points of the Lorenz map f_r, r^- and r^+, correspond to unstable periodic orbits of the full system. These points mark the boundaries of the chaotic invariant set. On the interval $[r^-, r^+]$, each branch of the map, $[r^-, d)$ and $(d, r^+]$, is stretched to cover the entire interval $[r^-, r^+]$. Using this interval as a Markov partition, we can define a hyperbolic Cantor set Λ, whose symbolic dynamics corresponds to sequences of left-right choices (as in the horseshoe mapping). Intuitively, the Cantor set Λ represents the "skeleton" of chaotic dynamics: although most trajectories eventually leave the set, the stretching and folding along the unstable direction preserves the essential sequence of left-right visits, capturing the underlying complexity of the full three-dimensional flow.

Meanwhile, the unstable fixed points q^- and q^+ of the map correspond to periodic trajectories that converge (as $r \to r_H$) to E_- and E_+, respectively. At this stage, although chaos exists on Λ, almost all trajectories eventually leave the chaotic set and settle to the stable equilibria. This regime is called preturbulence, illustrated in Figure 5.

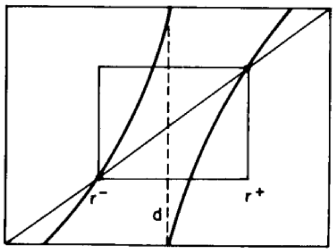

Figure 5: The map f_r, expanded in $[r^-, r^+]$ for $r_t < r < r_a$ (taken from [2]).

The bifurcation that turns the invariant set Λ of the preturbulent Lorenz flow into an attractor is subtle. As r increases, the fixed points r^- and r^+ of f_r move toward q^- and q^+, while the values of $f_r(d^-)$ and $f_r(d^+)$, the left and right limits of the map at the discontinuity d, move toward r^+ and r^-, respectively. A more detailed explanation of how the two-dimensional map $f_r : \Sigma \to \Sigma$ is reduced to the one-dimensional interval map $f_r : [q^-, q^+] \to [q^-, q^+]$ is given by Guckenheimer and Holmes (1983) in [2]. At the critical parameter $r = r_a \approx 24.06$, the map f_{r_a} sends the entire interval $[r^-, r^+]$ into itself. Consequently, any point starting in this interval remains trapped under iteration of the map and can no longer converge to the stable equilibria q^- or q^+. This self-mapping ensures that the chaotic dynamics in (r^-, r^+) persist for all time, effectively turning the preturbulent set Λ into the Lorenz strange attractor. For this parameter value the graph of f is illustrated in Figure 6.

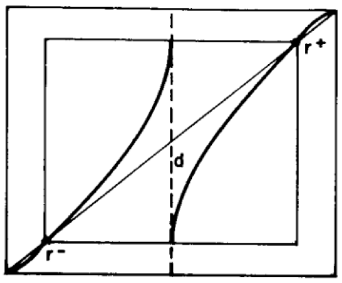

Figure 6: Another bifurcation for f_r: Λ becomes an attractor at $r = r_a$ (taken from [2]).

It is important to note that the Lorenz attractor appears before the subcritical Hopf bifurcation at $r = r_H$. The Hopf bifurcation removes the remaining stable equilibria, ending multistability, but it is not essential for the creation of the strange attractor.

When r increase for a last time, the periodic orbits correpsonding to $r^{\pm}$ collapse onto $q^{\pm}$ in the subcritical Hopf bifurcation at $r = r_H \approx 24.76$. A complex conjugate pair of eigenvalues crosses the imaginary axis, the equilibria lose stability, and the unstable periodic orbits r^- and r^+ collapse to $E_- = q^-$ and $E_+ = q^+$, respectively. Since the Hopf bifurcation is subcritical, no stable oscillations emerge, and trajectories are instead repelled into the already existing chaotic invariant set.

In conclusion, the Lorenz global attractor emerges through a series of bifurcations: first a local pitchfork bifurcation, then a local Hopf bifurcation followed by a homoclinic bifurcation creating preturbulence, and finally a global bifurcation that turns the chaotic set into an attractor. Despite being a three-dimensional system, its chaotic behavior can be largely understood through the dynamics of a one-dimensional expanding map, capturing the stretching, folding and left-right symbolic dynamics between the two lobes of the attractor. Which in the end leads to the well known Lorenz strange attractor. The Lorenz attractor is shown in all three coordinate planes (in Figure 7), with the xz-plane being the most widely recognized and commonly depicted view, a simulation illustrating the Lorenz System can be found in [6].

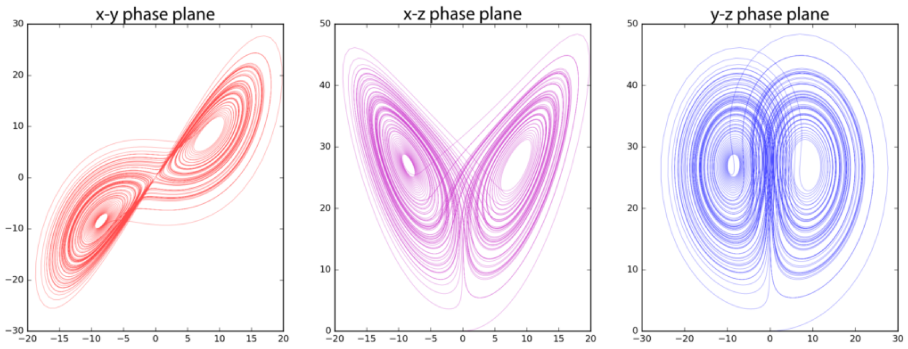

Figure 7: Lorenz attractor

5 Conclusion

We have studied the Lorenz-63 system to see how nonlinear differential equations can generate complex and chaotic dynamics. Originating from a simplified model of Rayleigh–Bénard convection, the Lorenz system captures key mechanisms underlying atmospheric instability and limited predictability.

We have first analyzed the equilibria of the system and their local stability. The equilibrium at the origin loses stability in a pitchfork bifurcation at $r = 1$, giving rise to two symmetrical equilibria. These equilibria are asymptotically stable for intermediate values of r, but lose stability at

$$r_H = \frac{\sigma(\sigma + b + 3)}{\sigma - b - 1}, \qquad \sigma > b + 1,$$

where a Hopf bifurcation occurs. By computing the first Lyapunov coefficient, we found that this Hopf bifurcation is always subcritical, implying that no stable periodic orbits are created and that the equilibria become unstable.

To understand the emergence of chaos, we considered global bifurcations of the system. Using a geometric approach based on one-dimensional return maps, we described how homoclinic bifurcations of the origin lead to the formation of a chaotic invariant set. As the parameter r increases further, this set becomes an attractor through a global bifurcation, giving rise to the Lorenz strange attractor. We noticed that this transition occurs before the Hopf bifurcation of the nontrivial equilibria, showing that chaos arises from global mechanisms rather than local oscillatory instabilities.

In conclusion, the Lorenz-63 system demonstrates how deterministic equations can exhibit unpredictable behavior due to high sensitivity to initial conditions. Through a combination of local bifurcation analysis and global geometric arguments, we have gained a clear understanding of how the iconic butterfly-shaped attractor emerges from simple nonlinear dynamics.

References

[1] L.P. Shilnikov, A.L. Shilnikov, D.V. Turaev, and L. Chua, *Methods of Qualitative Theory in Nonlinear Dynamics, Part II*, World Scientific, 2001, pp. 877–880.

[2] J. Guckenheimer and Ph. Holmes, *Nonlinear Oscillations, Dynamical Systems, and Bifurcations of Vector Fields*, Springer, 1983, Sections 6.4 and 5.7.

[3] Yu.A. Kuznetsov, O. Diekmann, and W.-J. Beyn, *Dynamical Systems Essentials*, On-line lecture notes, Section 6.7 (Exercise E 6.7.3), `http://www.staff.science.uu.nl/k̃ouzn101/NLDV/Lect12.pdf`.

[4] Yu.A. Kuznetsov, O. Diekmann, and W.-J. Beyn, *Dynamical Systems Essentials*, On-line lecture notes, Section 7.6, `http://www.staff.science.uu.nl/k̃ouzn101/NLDV/Lect14.pdf`.

[5] E. N. Lorenz biography, MacTutor History of Mathematics archive, St. Andrews: `https://mathshistory.st-andrews.ac.uk/Biographies/Lorenz`$_E dward/(accessed$ 2026). : $contentReference[oaicite:0]index=0$

[6] HighFellow, "Lorenz System with flot.js," online visualization of the Lorenz attractor: `https://highfellow.github.io/lorenz-attractor/attractor.html` (accessed 2026). :contentReference[oaicite:2]index=2

[7] A. E. Matouk, "Dynamical analysis, feedback control and synchronization of Liu dynamical system," *Nonlinear Analysis: Theory, Methods & Applications*, Vol. 69, No. 10, 2008, pp. 3213–3224.

[8] J. L. Kaplan and J. A. Yorke, "Preturbulence: A Flow With Zero Lyapunov Exponents," *Communications in Mathematical Physics*, Vol. 67, 1979, pp. 93–108.